

1. INTRODUCTION AND MODELS

The **El Niño / Southern Oscillation (ENSO)** is Earth's dominant year-to-year climate fluctuation, with impacts on economies and ecosystems worldwide. Predicting this phenomenon and projecting its future changes are key applications of global climate models, and the reliability of these outlooks depends on realistic simulations of ENSO.

SPEAR (*Seamless System for Prediction and Earth System Research*; Delworth et al. 2020), is a suite of coupled GCMs recently developed by NOAA GFDL. SPEAR uses the same core configuration as the GFDL CM4 & ESM4 models developed for CMIP6 (Held et al. 2019; Dunne et al. 2020), but is optimized to support seasonal-to-centennial climate research, forecasts, and projections. SPEAR contributes global seasonal forecasts to the North American Multi-Model Ensemble (NMME) each month.

The fast version of SPEAR (**SPEAR_LO**) uses the same 1° atmosphere & land grid as CM4, but coarsens the ocean & ice grids from 0.25° to 1° (telescoping to $\Delta y = 0.33^\circ$ near the equator). We have also developed **SPEAR_LO_FA**, which corrects climatological biases in the simulated SST, SSS, and wind stress by adding "flux adjustments" (FA) to the surface heat, salt, & momentum fluxes passed to the ocean (**Fig. 1**).

We examine **5-member ensemble simulations** from SPEAR_LO & SPEAR_LO_FA, run with **CMIP6 historical** forcings (1851-2014) and **SSP-585** projections (2015-2100). The ensembles are initialized in 1851 from a long **pre-industrial control run**. All obs & model datasets are regridded to a uniform $1^\circ \times 1^\circ$ grid prior to the analyses.

SPEAR_LO_FA flux adjustments (annual mean)

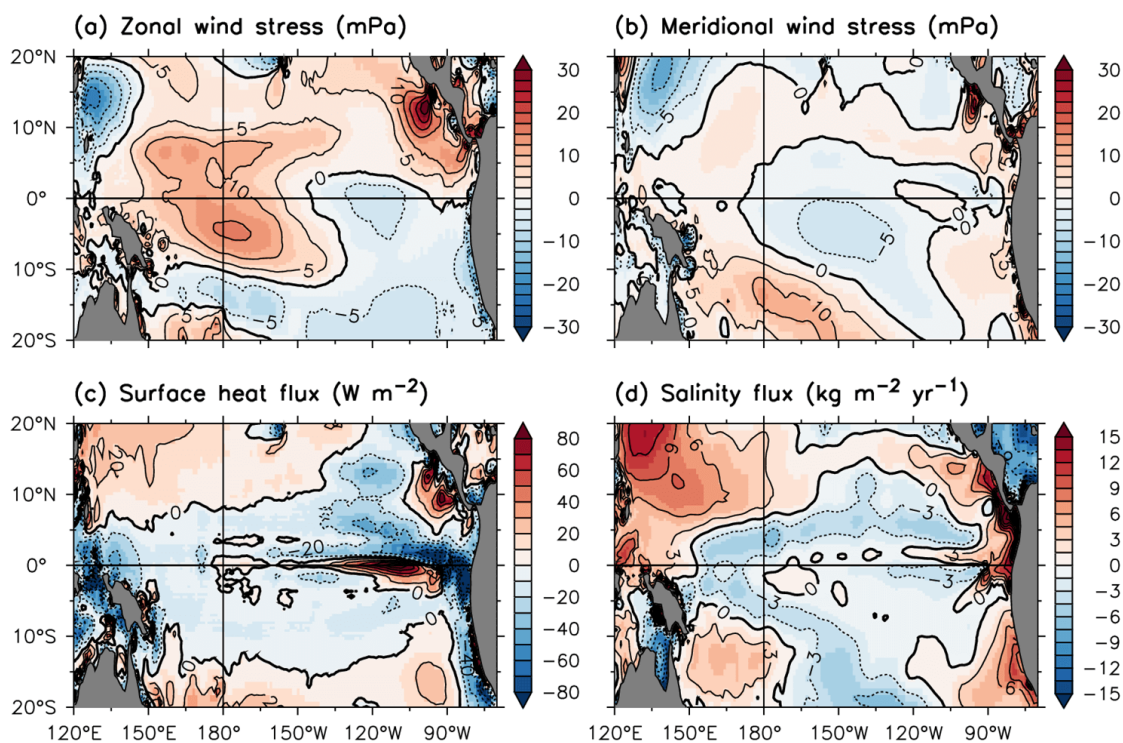


Fig. 1: Tropical Pacific annual means of the surface *flux adjustments* (FA) prescribed in SPEAR_LO_FA. The FA is seasonally-varying and interannually-repeating. Vector wind stress adjustments are applied over the global oceans (90°S - 65°N). Heat & salt adjustments are applied only over the tropical oceans (30°S - 30°N).

2. BACKGROUND CLIMATE

SPEAR_LO produces a very good simulation of tropical Pacific climate. Yet some biases are evident, including an equatorial cold tongue that is too cold & dry, a South American coastal zone that is too warm & wet, excessive rain in the west Pacific & ITCZ, a "double ITCZ" in the southeast tropical Pacific, equatorial trade winds that extend too far west, and an equatorial thermocline that is too shallow in the east (Figs. 2–6).

SPEAR_LO_FA corrects many of the remaining biases. The prescribed FA acts *directly* to weaken the equatorial cold tongue & trade winds, cool the SST near South America, and shift the west Pacific fresh pool eastward & equatorward. This improves the simulated climatological SST, and this *indirectly* improves the AGCM-simulated surface fluxes (which are further modified by the FA in Fig. 1, before entering the ocean). FA also improves the near-surface ocean temperatures & currents along the equator.

Even with FA however, a few biases remain in the AGCM's tropical rainfall, surface heat flux, and winds (Figs. 3c–5c) and in the OGCM's equatorial stratification (Fig. 6c). The FA results **target areas for future improvement** in the individual model components.

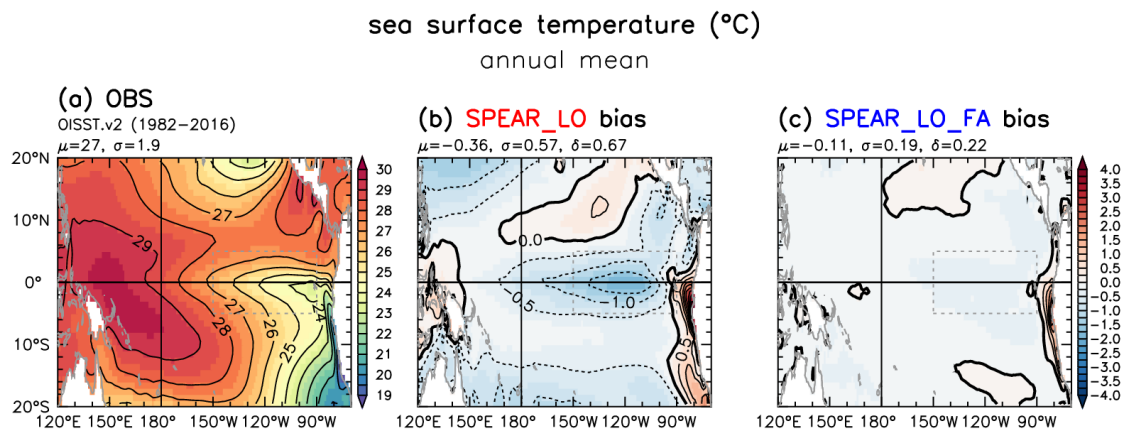


Fig. 2: (a) Observed annual-mean climatological SST (°C) from the OISST.v2 reanalysis (1982–2016). Also shown are the (b) SPEAR_LO and (c) SPEAR_LO_FA ensemble-mean annual-mean biases relative to (a) during 1980–2014. Gray dashed box is the NINO3 region (150°W–90°W, 5°S–5°N). The spatial mean (μ), standard deviation (σ), and RMS error (δ) are labeled above each panel.

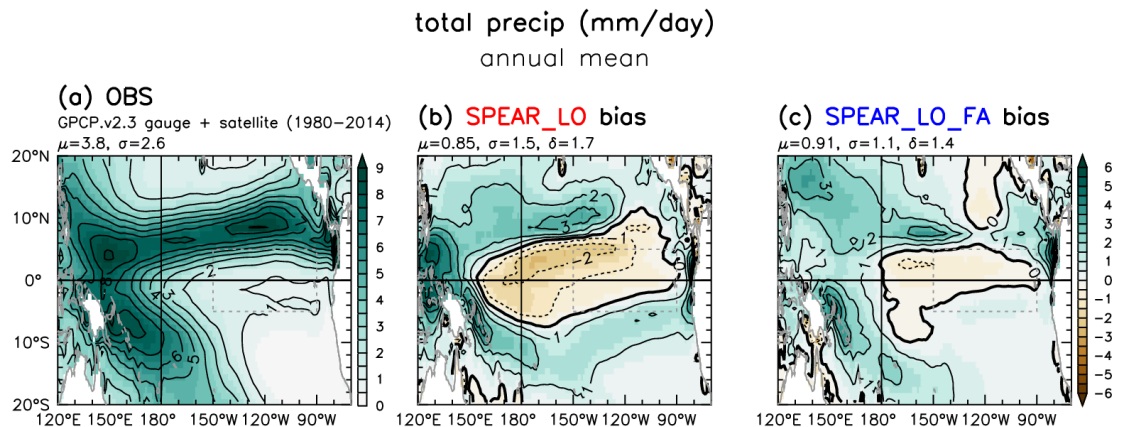


Fig. 3: As in Fig. 2, but for rainfall (mm day⁻¹). Obs are from GPCP.v2.3 (1980–2014).

net heat flux down at sfc (W/m^2)
annual mean

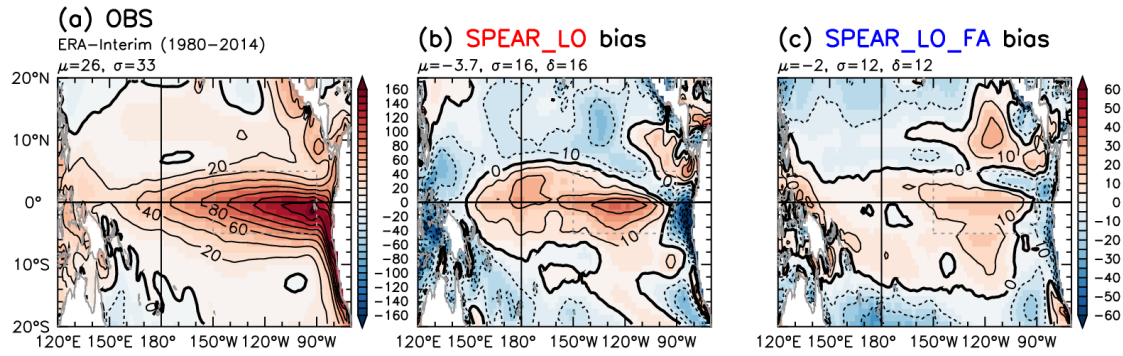


Fig. 4: As in Fig. 3, but for the net surface heat flux ($W m^{-2}$) into the ocean *before* any FA is applied. Obs are from the ERA-Interim reanalysis.

zonal wind stress (mPa)
annual mean

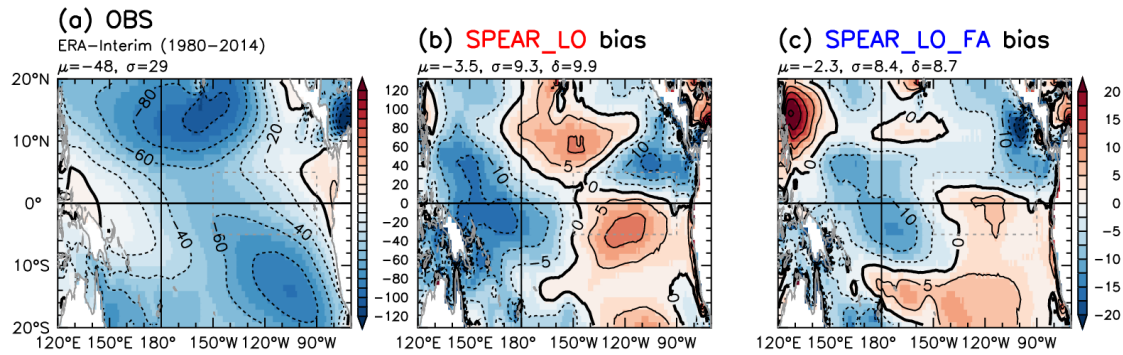


Fig. 5: As in Fig. 4, but for the surface zonal wind stress (mPa) on the ocean *before* any FA is applied.

temperature ($^{\circ}C, y=0$)
annual mean

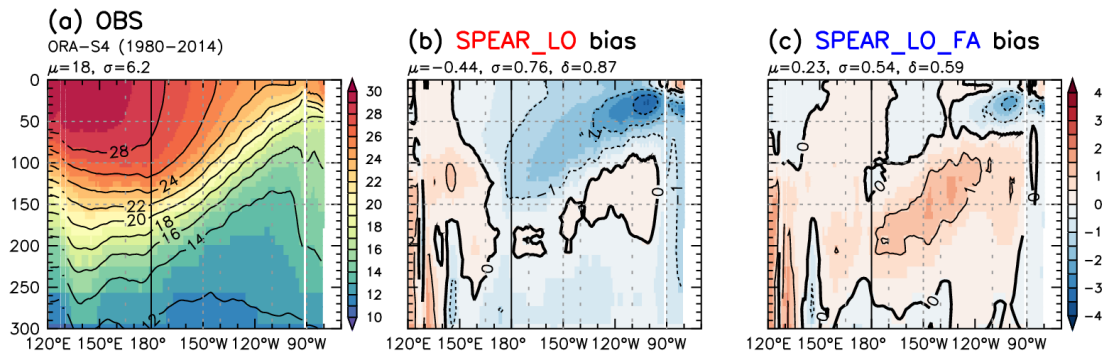


Fig. 6: As in Fig. 3, but for the subsurface temperature ($^{\circ}C$, top 300 m) along the equator. Obs are from the ORA-S4 reanalysis.

3. ENSO PERFORMANCE

SPEAR_LO produces a good simulation of ENSO, including the observed SST anomaly (SSTA) amplitude, period, spectrum, interdecadal modulation, seasonal synchronization, and remote teleconnections to the Pacific / North America (PNA) pattern (Figs. 7–11). But SPEAR_LO greatly underestimates the observed rainfall variance in the central equatorial Pacific (Fig. 12).

FA improves the ENSO simulation by weakening the SSTA variance in the western/central equatorial Pacific, lengthening the ENSO period, broadening ENSO's spectral peak, boosting the positive skewness of NINO3 SSTAs, strengthening the tendency of NINO3 SSTAs to peak in Nov–Dec, strengthening the rainfall variance in the central equatorial Pacific, and shifting the PNA pattern eastward and closer to the observed centers of action.

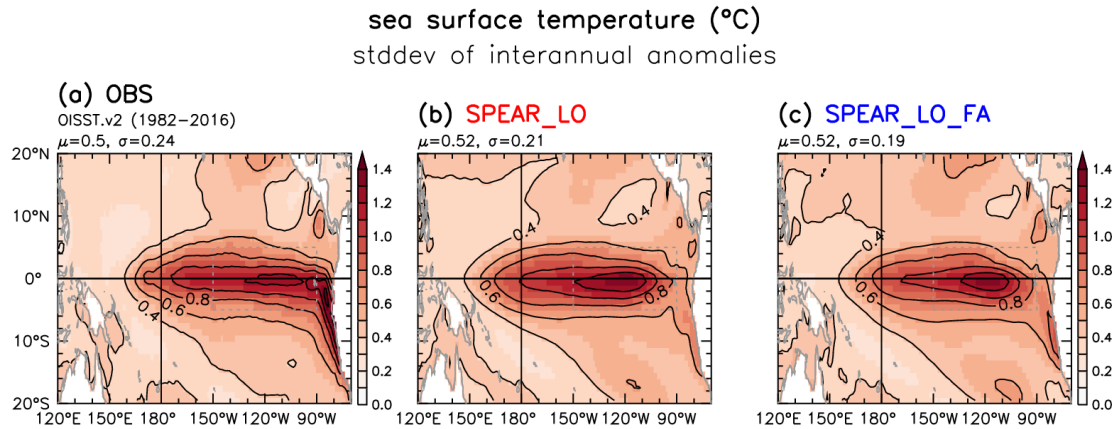


Fig. 7: Standard deviation of tropical Pacific interannual SSTAs (°C). (a) Obs from the OISST.v2 reanalysis (1982–2016). Also shown are the ensemble-mean standard deviation from the (b) SPEAR_LO and (c) SPEAR_LO_FA simulations during 1980–2014. All time series are first smoothed with a 9-month triangle that transmits (25, 50, 75)% amplitude at periods of (8, 11, 17) months.

Seasonality of ENSO events >1K

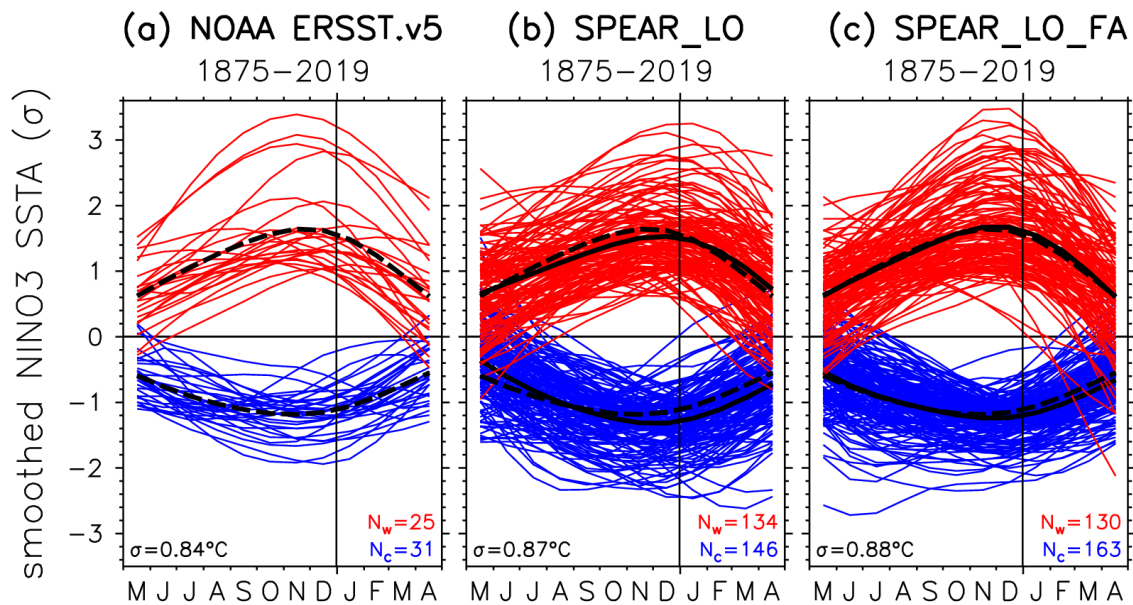


Fig. 8: Evolution of 7-month triangle-smoothed NINO3 SSTA (units of standard deviation σ , indicated at bottom left of each panel) during the May–April calendar year (abscissa), for the N_w warm events (red) and N_c cold events (blue) in the time series for which the smoothed NINO3 SSTA exceeds 1K during 1875–2019. (a) Obs from the ERSST.v5 reconstruction. Also shown are all events produced by the 5-member historical ensembles of (b) SPEAR_LO and (c) SPEAR_LO_FA during 1875–2019. Dashed black lines are the observed composite-mean warm & cold events from (a). Solid black lines are the corresponding simulated composite means.

Seasonality of ENSO events >1K

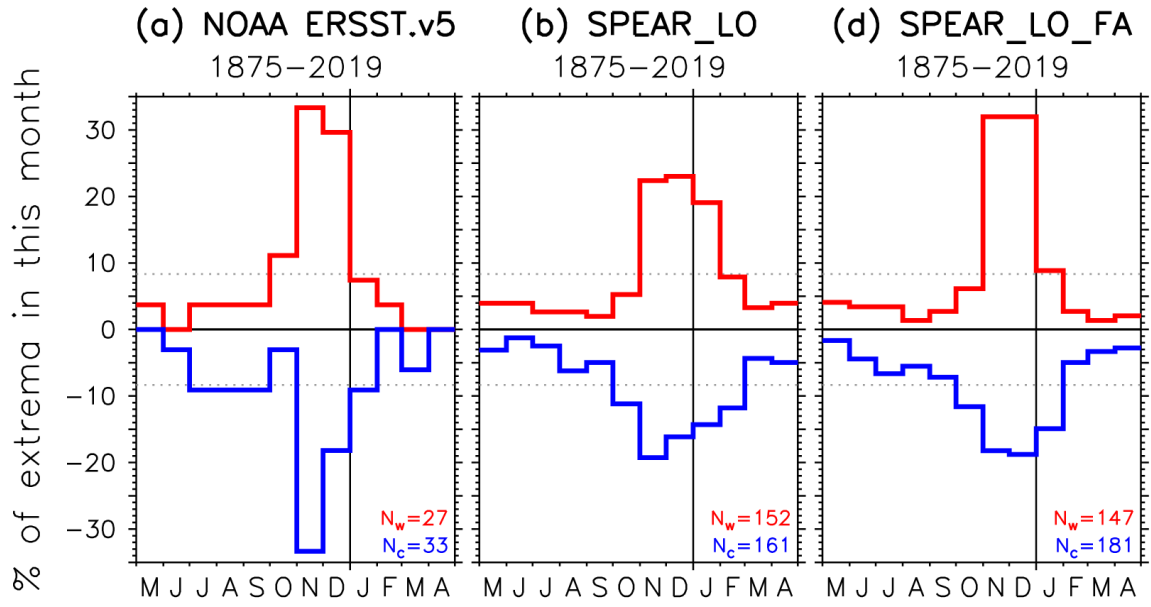


Fig. 9: Histograms of peak calendar months for the individual warm (red) and cold (blue) events in Fig. 8.

20yr-detrended DJF 200hPa height anomaly (m)
regressed on 20yr-detrended DJF NINO3 SSTA (K)

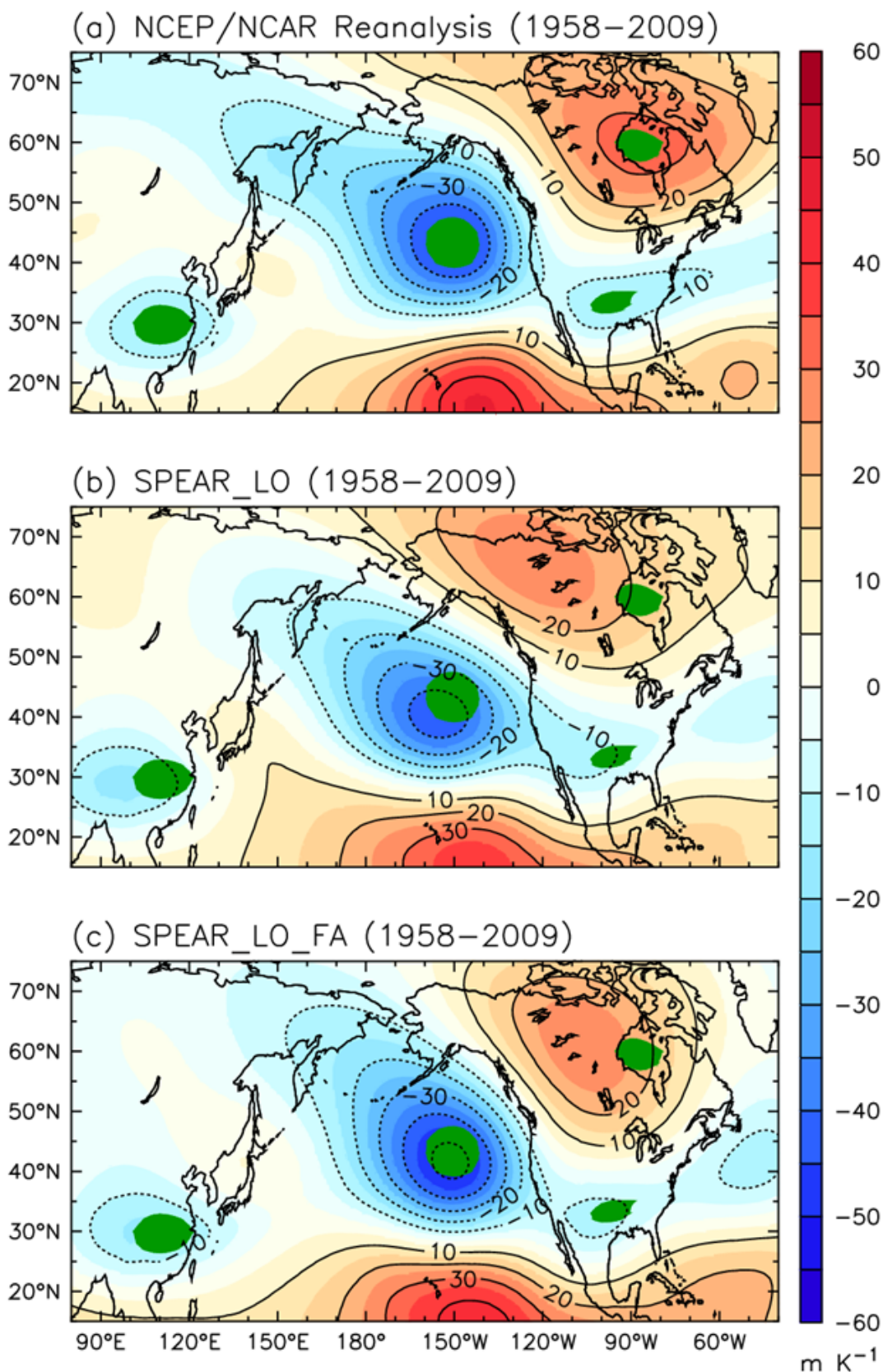


Fig. 10: DJF 200 hPa geopotential height anomalies regressed onto DJF NINO3 SSTAs ($m K^{-1}$) during 1958-2009. (a) Obs from the NCEP/NCAR reanalysis. Also shown are ensemble-mean regressions for (b) SPEAR_LO and (c) SPEAR_LO_FA. For reference, **green ellipses** indicate the observed extrema from (a). All time series are first detrended using a 211-month triangle high-pass smoother that transmits (75, 50, 25)% amplitude at periods of (15, 20, 30) years.

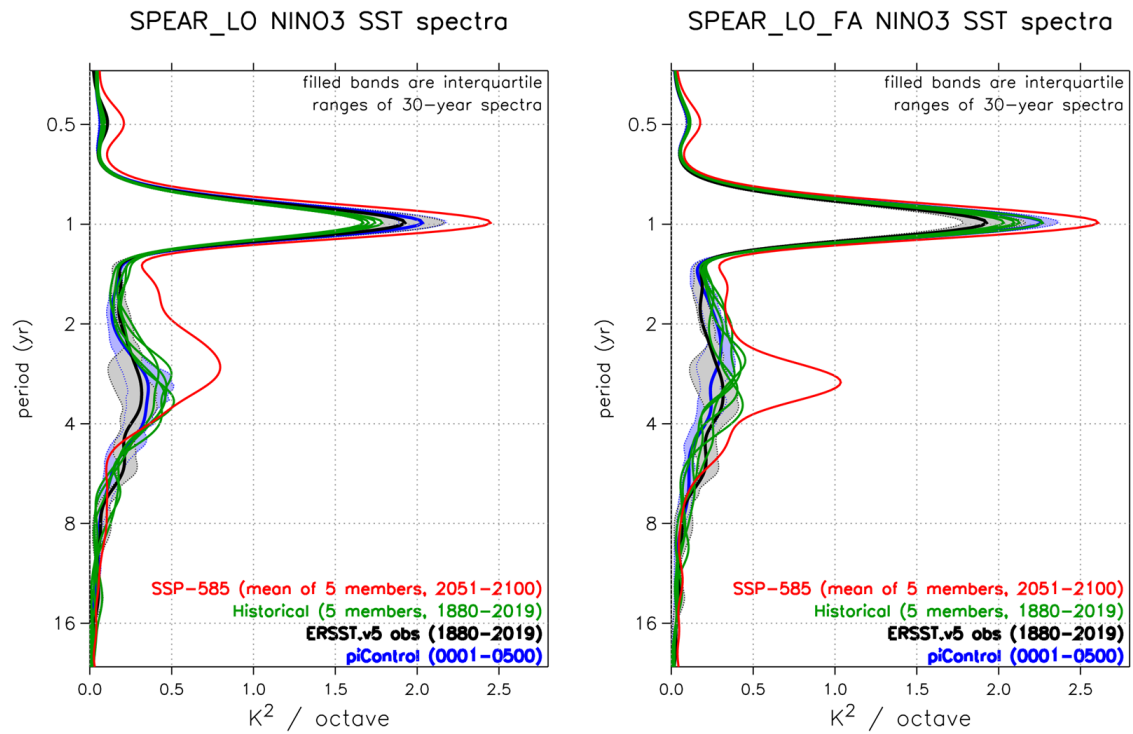


Fig. 11: Spectral power ($K^2 \text{ octave}^{-1}$) of NINO3 SST, as a function of period in octaves of the annual cycle, computed by time-averaging the spectral power density from a Morlet wavenumber-6 wavelet analysis. The area to the left of each curve represents the spectral power within a given frequency band. Thick **black** curve is the observed 120-yr-mean spectrum from ERSST.v5 (1880-2019). Gray shading is the min/max range of sliding 30-yr-mean spectra from the observations. Thick **green** curves are the corresponding spectra from the 5 historical ensemble members of SPEAR_LO (left panel) and SPEAR_LO_FA (right panel) during 1880-2019. Thick **blue** curve is a 500-yr-mean spectrum from a control run with fixed pre-industrial (1850) forcings, and blue shading is the range of sliding 30-yr-mean spectra from that control run. **Red** curve is the projected future ensemble-mean 50-yr-mean spectrum for 2051-2100.

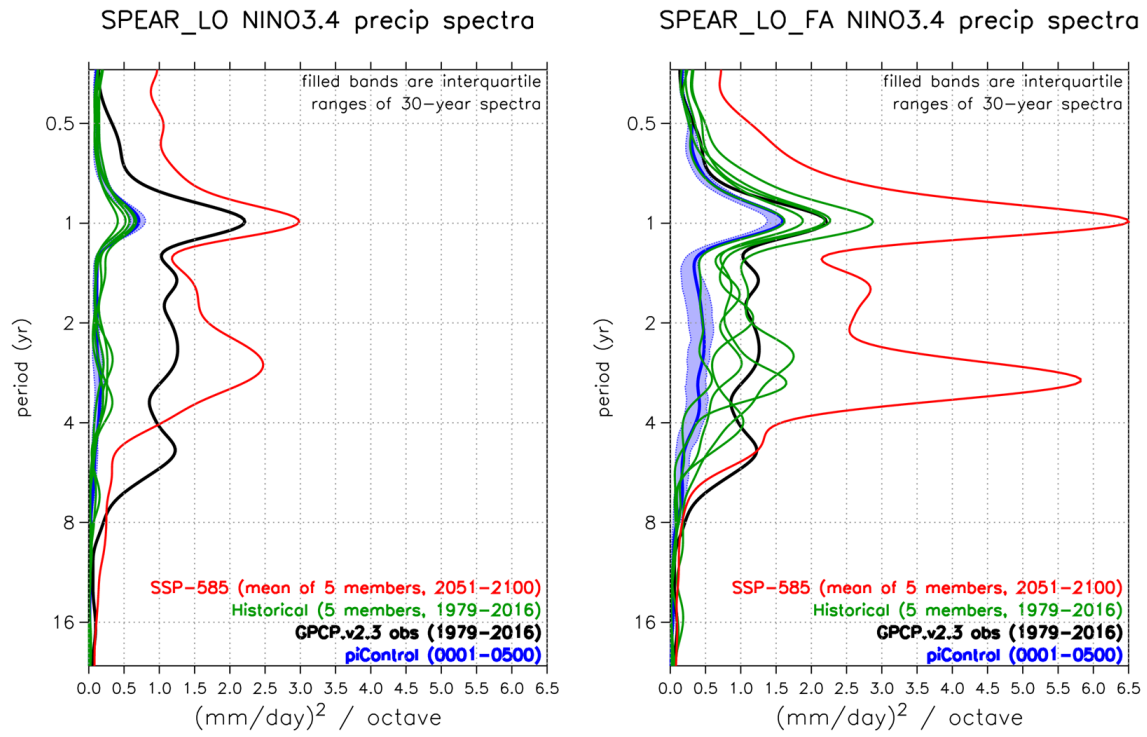


Fig. 12: As in Fig. 11, but for NINO3.4 rainfall ($\text{mm}^2 \text{day}^{-2} \text{octave}^{-1}$). Thick **black** curve is the observed 37-yr-mean spectrum from GPCP.v2.3 (1979-2016). Thick **green** curves are corresponding spectra from the 5 historical ensemble members during 1979-2016.

4. ENSO FEEDBACKS

SPEAR_LO's cold/dry bias along the equator (Figs. 2b–3b) inhibits its eastward & equatorward shifts of tropical Pacific convection, rainfall, and mid-tropospheric heating during El Niño (Fig. 13b) — with subsequent impacts on ENSO's key feedbacks & behavior (Figs. 14–19).

SPEAR_LO_FA improves the ENSO feedbacks by correcting the background climate biases. These changes:

- improve the remote **PNA** response (Fig. 10) by shifting the tropical rainfall & tropospheric heating anomalies eastward during El Niño (Fig. 13).
- enhance ENSO's **seasonal synchronization** and **warm / cold asymmetries** (Figs. 8–9), by strengthening links between the seasonal migration of the ITCZ & SPCZ and the equatorial air/sea wind coupling & noise (Choi et al. 2013, 2015).
- **attenuate ENSO SSTAs in the western/central equatorial Pacific** (Fig. 7b), by intensifying the convective cloud shading of SSTAs in that region (Fig. 14).
- strengthen the equatorial westerly wind stress response (τ_x') during El Niño (Fig. 15). This amplifies the role of anomalous thermocline depths, subsurface temperatures, and vertical thermal advection in the eastern equatorial Pacific (Figs. 17–18), reducing the westward **propagation** of SSTA (Fig. 16). The stronger τ_x' also boosts the meridional **recharge & discharge** of zonal-mean heat content during ENSO events (Fig. 19).
- meridionally broaden the τ_x' response to El Niño (Fig. 15). This slows the poleward recharge/discharge of equatorial heat content (Fig. 19), and lengthens the **ENSO period** (Fig. 11), consistent with Capotondi et al. (2006).

Both SPEAR_LO and SPEAR_LO_FA project a **future increase in extreme ENSO SST & rainfall anomalies** (Figs. 11–12). The FA version, whose stronger historical NINO3.4 rainfall variance is far more consistent with observations, projects a much *greater* absolute increase in NINO3.4 rainfall extremes. And while SPEAR_LO projects a shorter ENSO period for 2051-2100, SPEAR_LO_FA instead projects a *longer* period.

The **sensitivity of ENSO predictions & projections to model biases** in background climate highlights the need for caution when interpreting model-based outlooks (Stevenson et al. 2020; Ding et al. 2020). Efforts are underway at GFDL and within the international community to **diagnose, understand, & address these biases** and their impacts (Wittenberg et al. 2018; Ray et al. 2018; Planton et al. 2020, Guilyardi et al. 2020), and to **enhance the Tropical Pacific Observing System (TPOS)** to better support future model development (Cravatte et al. 2016; Kessler et al. 2019).

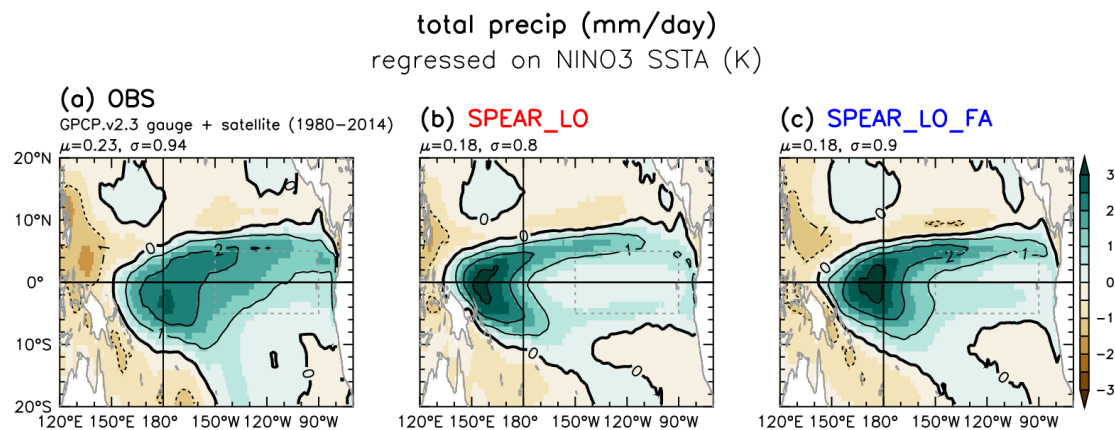


Fig. 13: Regression of monthly-mean tropical Pacific rainfall anomalies onto NINO3 SSTAs ($\text{mm day}^{-1} \text{K}^{-1}$) during 1980–2014. (a) Obs from GPCP.v2.3. Also shown are the ensemble-mean regressions from (b) SPEAR_LO and (c) SPEAR_LO_FA.

net heat flux down (W/m^2)
regressed on NINO3 SSTA (K)

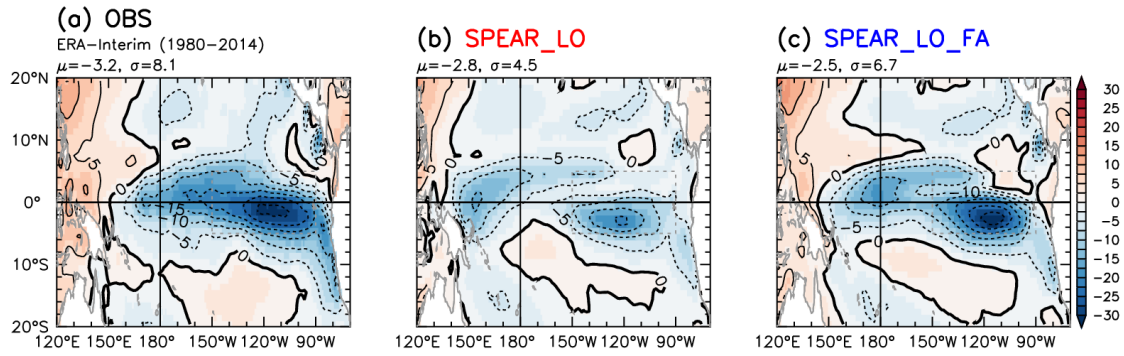


Fig. 14: As in Fig. 13, but for the net surface heat flux into the ocean ($W m^{-2} K^{-1}$). Obs are from the ERA-Interim reanalysis.

zonal wind stress (mPa)
regressed on NINO3 SSTA (K)

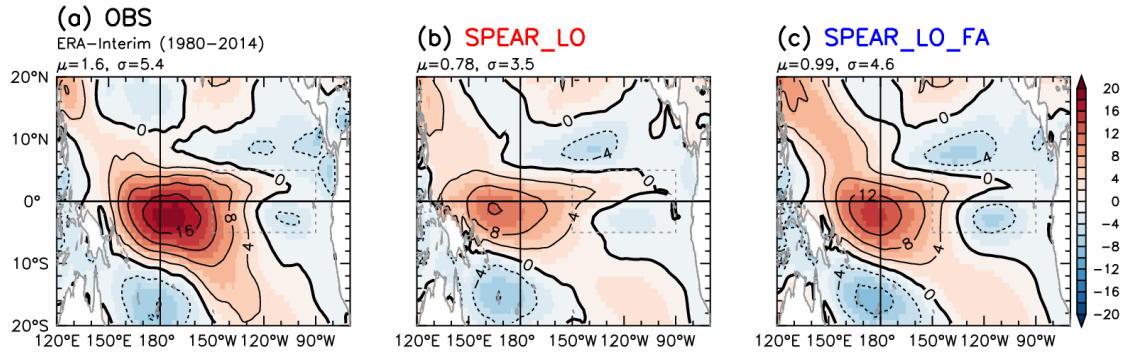


Fig. 15: As in Fig. 14, but for the zonal surface wind stress on the ocean ($mPa K^{-1}$).

sea surface temperature ($^{\circ}C$)
equator, lag-regressed on NINO3 SSTA (K)

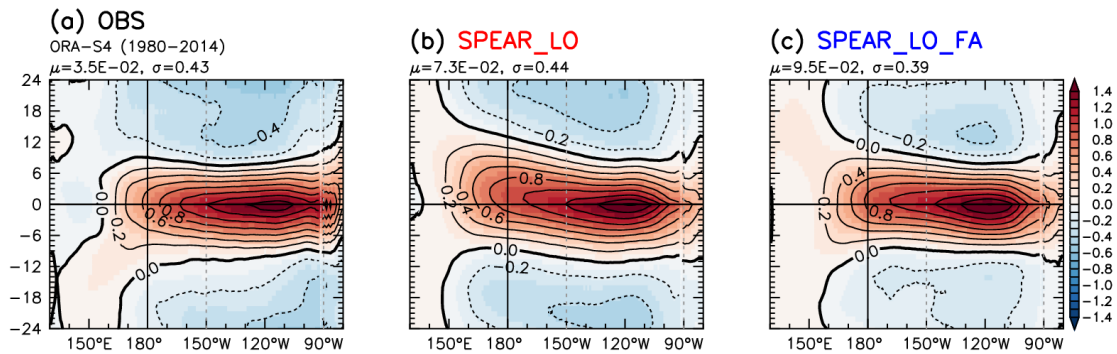


Fig. 16: Time vs. longitude plot of monthly-mean equatorial Pacific SSTAs regressed onto time-lagged NINO3 SSTAs ($K K^{-1}$) during 1980-2014. The ordinate is the lag time (in months) after the event's NINO3 SSTAs peak at lag 0; time evolves in the upward direction. (a) Obs from the ORA-S4 reanalysis. Also shown are the ensemble-mean lag-regressions from (b) SPEAR_LO and (c) SPEAR_LO_FA.

SST minus 50m temp (°C)
equator, lag-regressed on NINO3 SSTA (K)

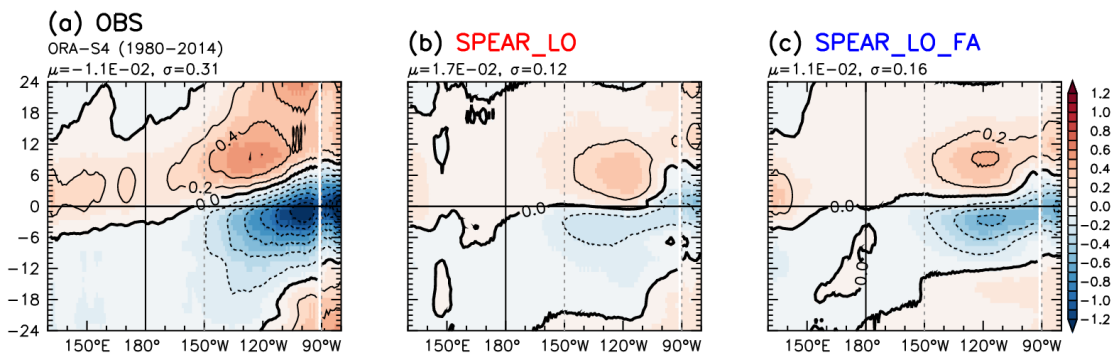


Fig. 17: As in Fig. 16, but for the anomalous near-surface thermal stratification (defined as SST minus 50 m temperature) regressed on NINO3 SSTA.

3d-advect htg from uvwT (K/year, z=0:50@ave)
equator, lag-regressed on NINO3 SSTA (K)

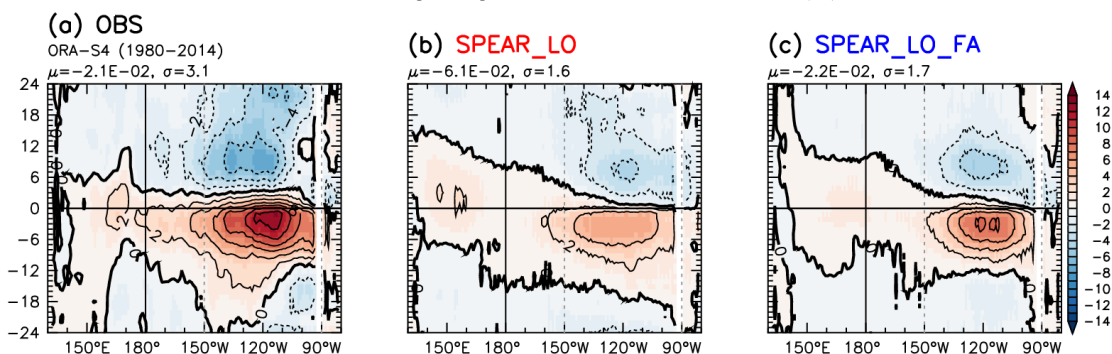


Fig. 18: As in Fig. 16, but for anomalous 3-dimensional thermal advection ($K yr^{-1}$) averaged over the top 50 m of the ocean. The total advection is computed as a product of the monthly-mean currents and monthly-mean temperature gradients. A 12-month climatology is then subtracted to yield the advection anomalies, which are then regressed against the lagged NINO3 SSTA.

temperature (°C, z=0.0:300.0@ave)
Pacific zonal mean, lag-regressed on NINO3 SSTA (K)

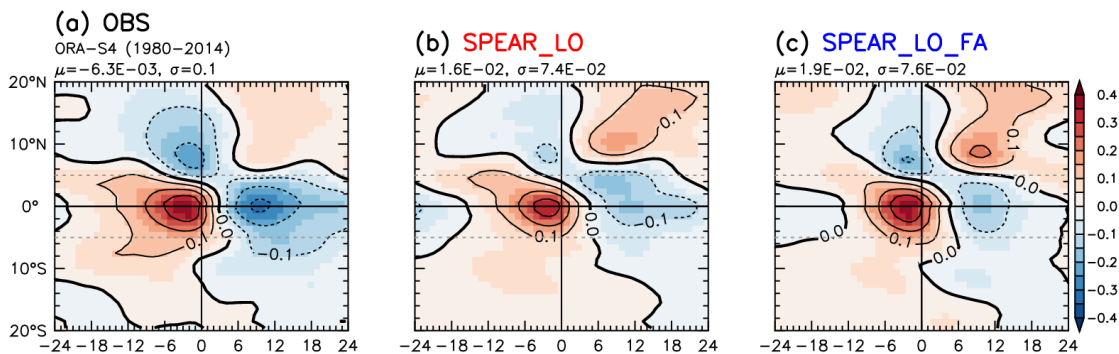


Fig. 19: Latitude vs. time plot of monthly-mean equatorial Pacific zonal-mean upper-ocean heat content anomalies regressed onto time-lagged NINO3 SSTAs ($K K^{-1}$) during 1980-2014. The heat content is computed as the temperature averaged over the top 300 m of the ocean. The abscissa is the lag time (in months) after the event's NINO3 SSTAs peak at lag 0; time evolves in the rightward direction. (a) Obs from the ORA-S4 reanalysis. Also shown are the ensemble-mean lag-regressions from (b) SPEAR_LO and (c) SPEAR_LO_FA.

DISCLOSURES

*Additional members of the SPEAR Model Development Team:

Alistair Adcroft, Mitchell Bushuk, Jan-Huey Chen, Krista A. Dunne, Paul A. Ginoux, Rich Gudgel, Nathaniel Johnson, Robert Hallberg, Lucas Harris, Matthew Harrison, Sarah B. Kapnick, Shian-Jiann Lin, Feiyu Lu, Sergey Malyshev, Chris Milly, Hiroyuki Murakami, Vaishali Naik, Salvatore Pascale, David Paynter, Anthony Rosati, Daniel Schwarzkopf, Elena Shevliakova, Seth Underwood, Baoqiang Xiang, Xiaosong Yang, Honghai Zhang, Liping Zhang, Ming Zhao

ABSTRACT

We assess the dynamics of the El Niño / Southern Oscillation (ENSO) as simulated in the SPEAR_LO global coupled GCM, recently developed by NOAA's Geophysical Fluid Dynamics Laboratory (GFDL). SPEAR_LO supports seasonal-to-centennial climate research, forecasts, and projections, and contributes routine seasonal forecasts as part of the North American Multi-Model Ensemble (NMME). Compared to its predecessors, SPEAR_LO simulates improved ENSO patterns, spectra, seasonal timing, teleconnections, and ocean-atmosphere feedbacks. Analyses of the upper-ocean heat budget and ocean-atmosphere feedbacks illustrate how SPEAR's improved physical formulations contribute to more realistic simulations of the tropical Pacific climatology and ENSO. Further correcting the tropical climatology — via flux-adjustments of the model SST, SSS, and surface wind stress — yields an even better simulation of ENSO, and illuminates the roles of the background state in ENSO dynamics and feedbacks. Promising avenues toward future model improvements are discussed, along with implications for the Tropical Pacific Observing System (TPOS) and community-developed metrics to assess ENSO in climate models.

REFERENCES

- Capotondi, A., A. Wittenberg, and S. Masina, 2006: Spatial and temporal structure of tropical Pacific interannual variability in 20th century coupled simulations. *Ocean Modelling*, 15, 274-298. <http://doi.org/10.1016/j.ocemod.2006.02.004> (<http://doi.org/10.1016/j.ocemod.2006.02.004>)
- Choi, K.-Y., G. A. Vecchi, and A. T. Wittenberg, 2013: ENSO transition, duration and amplitude asymmetries: Role of the nonlinear wind stress coupling in a conceptual model. *J. Climate*, 26, 9462-9476. <https://doi.org/10.1175/JCLI-D-13-00045.1> (<https://doi.org/10.1175/JCLI-D-13-00045.1>)
- Choi, K.-Y., G. A. Vecchi, and A. T. Wittenberg, 2015: Nonlinear zonal wind response to ENSO in the CMIP5 models: Roles of the zonal and meridional shift of the ITCZ/SPCZ and the simulated climatological precipitation. *J. Climate*, 28, 8556-8573. <http://doi.org/10.1175/JCLI-D-15-0211.1> (<http://doi.org/10.1175/JCLI-D-15-0211.1>)
- Cravatte, S., et al., 2016: First Report of TPOS 2020. GOOS-215, 200 pp. Available online at: <http://tpos2020.org/first-report> (<http://tpos2020.org/first-report>) <http://doi.org/10.13140/RG.2.2.28674.07363> (<http://doi.org/10.13140/RG.2.2.28674.07363>)
- Delworth, T. L., et al., 2020: SPEAR: The next generation GFDL modeling system for seasonal to multidecadal prediction and projection. *J. Adv. Model. Earth Syst.*, 12 (3), e2019MS001895. <http://doi.org/10.1029/2019MS001895> (<http://doi.org/10.1029/2019MS001895>)
- Ding, H., M. Newman, M. A. Alexander, and A. T. Wittenberg, 2020: Relating CMIP5 model biases to seasonal forecast skill in the tropical Pacific. *Geophys. Res. Lett.*, 47 (5), e2019GL086765. <http://doi.org/10.1029/2019GL086765> (<http://doi.org/10.1029/2019GL086765>)
- Dunne, J. P., et al., 2020: The GFDL Earth System Model version 4.1 (GFDL-ESM4.1): Overall coupled model description and simulation characteristics. *J. Adv. Model. Earth Syst.*, 12 (11), e2019MS002015. <http://doi.org/10.1029/2019MS002015> (<http://doi.org/10.1029/2019MS002015>)
- Fedorov, A., S. Hu, A. T. Wittenberg, A. Levine, and C. Deser, 2020: ENSO low-frequency modulations and mean state interactions. Chapter 8 of: *El Niño Southern Oscillation in a Changing Climate*, American Geophysical Union, Washington, DC, pp. 173-198. <http://doi.org/10.1002/9781119548164.ch8> (<http://doi.org/10.1002/9781119548164.ch8>)
- Guilyardi, E., A. Capotondi, and M. Lengaigne, S. Thual, and A. T. Wittenberg, 2020: ENSO modeling: History, progress, and challenges. Chapter 9 of: *El Niño Southern Oscillation in a Changing Climate*, American Geophysical Union, Washington, DC, pp. 201-226. <http://doi.org/10.1002/9781119548164.ch9> (<http://doi.org/10.1002/9781119548164.ch9>)
- Held, I. M., et al., 2019: Structure and performance of GFDL's CM4.0 climate model. *J. Adv. Model. Earth Syst.*, 11 (11), 3691-3727. <http://doi.org/10.1029/2019MS001829> (<http://doi.org/10.1029/2019MS001829>)
- Kessler, W. S., et al., 2019: Second Report of TPOS 2020. GOOS-234, 265 pp. Available online at: <http://tpos2020.org/project-reports/second-report> (<http://tpos2020.org/project-reports/second-report>) <http://doi.org/10.13140/RG.2.2.17161.29289> (<http://doi.org/10.13140/RG.2.2.17161.29289>)
- Planton, Y., E. Guilyardi, A. T. Wittenberg, J. Lee, P. J. Gleckler, et al.: Evaluating climate models with the CLIVAR 2020 ENSO metrics package. *Bull. Amer. Meteorol. Soc.*, in press. <http://doi.org/10.1175/BAMS-D-19-0337.1> (<http://doi.org/10.1175/BAMS-D-19-0337.1>)
- Ray, S., A. T. Wittenberg, S. M. Griffies, and F. Zeng, 2018: Understanding the equatorial Pacific cold tongue time-mean heat budget, Part I: Diagnostic framework. *J. Climate*, 31 (24), 9965-9985. <http://doi.org/10.1175/JCLI-D-18-0152.1> (<http://doi.org/10.1175/JCLI-D-18-0152.1>)
- Stevenson, S., A. T. Wittenberg, J. Fasullo, S. Coats, and B. Otto-Bliesner: Understanding diverse model projections of future extreme El Niño. *J. Climate*, in press. <http://doi.org/10.1175/JCLI-D-19-0969.1> (<http://doi.org/10.1175/JCLI-D-19-0969.1>)
- Wittenberg, A. T., et al., 2018: Improved simulations of tropical Pacific annual-mean climate in the GFDL FLOR and HiFLOR coupled GCMs. *J. Adv. Model. Earth Syst.*, 10 (12), 3176-3220. <http://doi.org/10.1029/2018MS001372> (<http://doi.org/10.1029/2018MS001372>)